

THE REDDENING TOWARDS CASSIOPEIA A'S SUPERNOVA: CONSTRAINING THE ⁵⁶Ni YIELD

KRISTOFFER A. ERIKSEN¹, DAVID ARNETT, DONALD W. MCCARTHY
Steward Observatory, University of Arizona, Tucson, AZ 85721

AND

PATRICK YOUNG
School of Earth and Space Exploration, Arizona State University, Tempe, AZ, 85287
Draft version October 30, 2018

ABSTRACT

We present new reddening measurements towards the young supernova remnant Cassiopeia A, using two techniques not previously applied to this object. Our observations of the near-infrared [Fe II] 1.257 μ m and 1.644 μ m lines show the extinction to be highly variable across the remnant, increasing towards the west and the south, consistent with previous radio and X-ray observations. While the absolute value of A_V as determined by the [Fe II] lines is uncertain due to conflicting calculations and observations of their intrinsic flux ratio, parts of the remnant without previous optical measurements show comparatively higher reddening. We find $A_V = 6.2 \pm 0.6$ from the broadband shape of the infrared synchrotron emission of a knot within 13'' of the expansion center. Given this reddening, the apparent faintness of the nascent supernova, and iron mass constraints from X-ray observations, we estimate an ejected mass of ⁵⁶Ni of 0.058 – 0.16 M_{\odot} . Taken with γ -ray observations of the ⁴⁴Ti decay chain, this nickel mass is broadly consistent with the solar ⁴⁴Ca/⁵⁶Fe ratio.

Subject headings: supernova remnants — supernovae: individual (SN1680) — dust, extinction — nuclear reactions, nucleosynthesis, abundances

1. INTRODUCTION

Cassiopeia A is the remnant of one of the most recent known supernova in the Galaxy. It is the prototype of the “oxygen-rich” class of supernova remnants (OSNRs), whose optical spectra are dominated by highly Doppler shifted lines of oxygen and other advanced burning products, but are nearly devoid of hydrogen and helium. Because these remnants have not yet swept up significant interstellar material, their abundance pattern reflects that of their progenitor star and supernova. As such, the OSNRs, and Cas A in particular, allow unparalleled access to the physics of massive stars and supernova, and should provide tight constraints on models of nucleosynthesis, stellar mixing, supernova physics, and ISM enrichment.

Given its distance (3.4^{+0.3}_{-0.1} kpc, Reed et al. 1995), circumpolar location in the northern sky, and the most quoted reddening towards Cas A ($A_V \sim 5$, Hurford & Fesen 1996, hereafter HF96), it is surprising that its nascent supernova was largely unreported. SN1604 (Kepler’s SN), SN1572 (Tycho’s SN), SN1054 (the Crab Nebula) and SN1006 were all widely observed and recorded by contemporary astronomers in Europe, the Far East, or both. Cas A was not. While Flamsteed may have seen the event as a 6th magnitude optical transient in 1680 (Ashworth 1980, though Kamper 1980 provides a dissenting opinion), it was certainly less remarkable than other historical Galactic supernovae. Why? Was the Cas A supernova an unusual, under-luminous event? Were contemporary observers unlucky, and the supernova at peak brightness was highest in the northern sky during

daylight? Is the extinction towards Cas A greater than previously assumed?

Aside from this historical oddity, the apparent faintness of Cas A’s outburst presents an astrophysical conundrum. The peak luminosity and characteristic light curve of supernovae are driven by energy injected into the expanding stellar debris by the radioactive decay of ⁵⁶Ni and its daughter nucleus ⁵⁶Co. Thus, the peak brightness is proportional to the ejected mass of ⁵⁶Ni. Since the complete explosive silicon burning that produces radioactive nickel takes place in the deepest layers of the supernova, the nickel yield is intimately linked with the explosion mechanism, energy, mass cut, and fall-back fraction. Its diagnostic power is further enhanced when compared to a supernova’s ⁴⁴Ti yield. This trace isotope is produced by “ α -rich freeze-out,” a process of incomplete silicon burning that dominates in regions of higher entropy (i.e. lower density). The high ⁴⁴Ti abundance, as determined by γ -radiation observations of its decay chain (Iyudin et al. 1994, Vink et al. 2001) relative to the implied ⁵⁶Ni mass inferred from Cas A’s apparently faint outburst, are inconsistent with yields expected from symmetric explosion calculations (Timmes et al. 1996). This is generally assumed to be evidence for asymmetry in the supernova (e.g. Nagataki et al. 1998). Therefore, tighter measurements of ⁴⁴Ti/⁵⁶Ni should provide helpful constraints on advanced supernova explosion calculations. Furthermore, ⁴⁴Ti appears to be produced exclusively in core collapse and sub-Chandrasekhar mass SNIa (Timmes et al. 1996). A measurement of radioactive titanium and nickel in Cas A may inform Galactic chemical evolution and stellar population synthesis models in determining the relative importance of these two types of supernovae in producing the observed solar abundance ratio of ⁴⁴Ca/⁵⁶Fe, the two stable daughter

¹ Visiting Astronomer, Kitt Peak National Observatory. KPNO is operated by AURA, Inc. under contract to the National Science Foundation.

products of these nuclei.

Thus a proper inventory of ^{56}Ni or, equivalently ^{56}Fe , in Cas A is desirable. Willingale et al. (2003), using XMM-Newton X-ray observations, find an X-ray emitting iron mass (presumably dominated by ^{56}Fe) of $0.058M_{\odot}$. Because the cooling time of the X-ray emitting plasma is generally longer than the age of the supernova remnant, this is, to a good approximation, the sum total of iron that has been heated to X-ray emitting temperatures upon passage through the reverse shock. However, it does not include denser material that retained enough electrons to cool efficiently through EUV, optical, and infrared emission. The cooling times for these plasmas can be weeks or months, making a full inventory of gas of these densities at reverse shock passage difficult. Similarly, material that has not yet encountered the reverse shock is nearly invisible.

Here we take a different approach and attempt to bound the allowed total mass of ejected ^{56}Ni . Given that Cas A's SN was apparently unremarkable at Earth, knowledge of the extinction towards the supernova, a distance measurement, and a limit on the apparent magnitude place constraints on the intrinsic peak luminosity of the event. Previous optical measurements of the reddening suffer from a selection effect, in that the most common method for estimating A_V is infeasible in regions of higher extinction. Existing CO (Troland et al. 1985) and X-ray (e.g. Keohane et al. 1996) observations show the absorption to Cas A to be spatially variable, with a general trend of increasing extinction from east to west, though poor spatial resolution washes out structure on scales smaller than the beam and will underestimate A_V if the absorbers are clumped. Indeed, interferometric observations of H_2CO absorption towards Cas A (Reynoso & Goss 2002) show considerable clumpiness. Moreover, radio and X-ray measurements of the absorbing column require an assumed gas to dust ratio to convert to optical extinction. As such, existing estimates of the reddening span several magnitudes, most commonly $A_V \sim 4 - 8$. (Fesen et al. 2006 assume $A_V = 6 - 8$ towards the compact remnant.) These uncertainties have limited the accuracy of previous attempts (e.g. Troland et al. 1985) to use the peak brightness to constrain the properties of the supernova. Here we present significantly improved measurements of A_V using [Fe II] infrared emission lines and a new technique based on measurement of the infrared spectral index of the synchrotron emission of Cas A.

The rest of the paper is organized as follows. In §2, we detail the new near-infrared images and spectroscopy and the archival mid-infrared imaging we use for our measurements. In §3 we address the challenges of measuring the extinction towards Cas A with emission lines, estimate A_V from our [Fe II] observations, and describe and present results from our measurement of the infrared synchrotron emission. In §4, we bound the ejected nickel mass and discuss its implications. §5 is a summary of our results.

2. OBSERVATIONS

2.1. Near-Infrared Imaging

We imaged Cas A with the PISCES (McCarthy et al. 2001) near-infrared camera attached to the Steward Observatory 2.3-meter Bok telescope, over two different runs

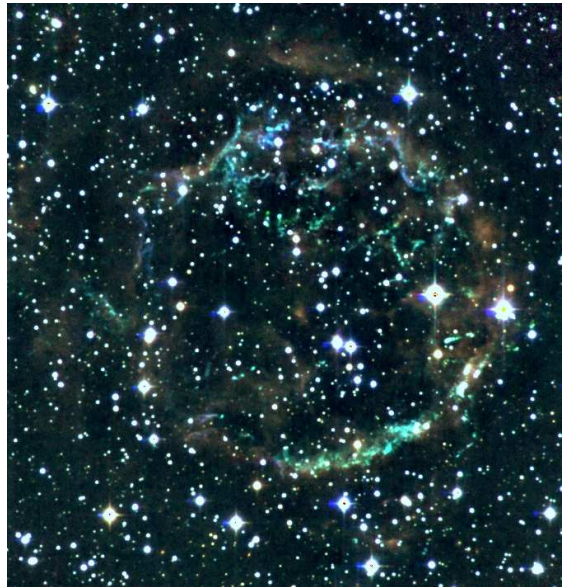


FIG. 1.— Our color JHK_s (red, green, blue) PISCES image of Cassiopeia A. The clumpy blue/green features are line emission from shock heated ejecta and circumstellar material, while the smoother red features are synchrotron emission. Synchrotron “Knot N” from Wright et al. (1999) is clearly visible as a diffuse red feature near the center of the remnant.

in summer 2002 and 2003. The 8.5 circular field of view and 0.75 pixels at the Bok f/9 focus allowed us to image the entire remnant in a single pointing while adequately sampling typical Kitt Peak seeing, which ranged from $0.8-1.5$. All observations were made with broadband filters from the 2MASS system.

In July 2002, we used a 3×3 dither pattern, with 60 second individual exposures in J , and 30 second exposures in H . The total exposure times were 54 minutes in J and 40 minutes in H . In July 2003, we used a similar strategy, observing Cas A in J (45s individual, 45 minute total exposure), H (12s individual, 35 minutes total exposure) and K_s (10s individual, 56 minutes total exposure).

Standard image processing, including dark subtraction, flat-fielding, distortion correction, and image stacking were accomplished with the IRAF² package. For the 2002 run, flat-field frames were constructed from median-filtered off-source dithers interspersed with on-source pointings. In 2003, no off-source pointings were taken, and flats were made from source frames. This resulted in a poor quality flat-field, and an underestimation of the flux in low-surface brightness, high-coverage features like the diffuse synchrotron emission observed in all bands. As such, the 2003 J and H images were not used for flux measurements, though they were used to estimate a correction factor for the 2003 K_s data. Magnitude calibration was achieved by comparison with 2MASS (Skrutskie et al. 2006) stars in the observed field.

We present in Figure 1 a color JHK_s image of Cas A from our PISCES data. The clumpy shocked material has strong lines in the J and H bands and appears blue-green, while the K_s image is dominated by smoother synchrotron continuum. While this non-thermal emis-

² IRAF is distributed by the National Optical Astronomy Observatory, which is operated by the Association of Universities for Research in Astronomy (AURA) under cooperative agreement with the National Science Foundation.

sion is detected in all bands, it is strongest at longer wavelengths, and displays red.

2.2. Near-Infrared Spectroscopy

Using our *J* band image to target knots of interest, we observed four slit positions on 26-27 September 2004 with the FLAMINGOS³ multi-object spectrograph on the KPNO 4-meter telescope. The JH grism and 6 pixel wide long-slit provided simultaneous wavelength coverage from approximately 0.95-1.8 μ m across a $10' \times 1.9''$ slit on the sky, and delivered approximately 25 \AA resolution across the J and H bands. The emission knots in Cas A are densely packed on the sky, so it was impossible to use the standard $10''$ nod along the slit for sky subtraction. Since the FLAMINGOS slit is approximately twice as long as the diameter of Cas A's bright ring, we placed the all supernova remnant line emission at one end of the slit, and used a $5'$ nod. While this large throw cost extra overhead (including reacquisition of a guide star at each nod), it ensured knots of interest would not overlap between nods. Utilizing an "AABB" pattern, each individual exposure was 300 seconds, for a total A+B on-source exposure time of 4800-6600 seconds.

Standard near-infrared spectroscopic reductions (dark subtraction, flat-fielding, sky subtraction, distortion correction) were accomplished with a combination of IRAF and custom Perl Data Language⁴ (Glazebrook & Economou 1997) scripts. For the J band, we set the wavelength calibration with HeNeAr lamps. H band wavelength calibration was made against the night sky lines, using VLT/NIRMOS OH line list and sky spectrum convolved to our resolution (Rousselot et al. 2000). The instrumental throughput and telluric transmission was measured with observations of the nearby G2V star HD212809, divided by the synthetic solar spectrum included with the spectral synthesis code SPECTRUM v2.73 (Gray & Corbally 1994). Small corrections to the shape of the instrumental response were corrected with observations of the A0V star HD240290, relative to a synthetic Vega spectrum calculated with the same code. Finally, the absolute flux scale was set with an observation of G191B2B, utilizing the STIS/NICMOS fluxes (Bohlin 2007).

2.3. Spitzer Mid-Infrared Imaging

We used archival *Spitzer*/IRAC images of Cas A originally presented by Ennis et al. (2006). While data exists for all four IRAC bands, the broader point spread function for the longer wavelengths degrades our ability to disentangle the synchrotron emission peaks from both the emission-line emitting regions and the smooth continuum background, so we limit our analysis to channels 1 & 2 (3.6 μ m & 4.5 μ m, respectively). Data products were downloaded from the archive, processed and mosaicked using standard IRAC processing.

³ FLAMINGOS was designed and constructed by the IR instrumentation group (PI: R. Elston) at the University of Florida, Department of Astronomy, with support from NSF grant AST97-31180 and Kitt Peak National Observatory

⁴ The Perl Data Language (PDL) has been developed by K. Glazebrook, J. Brinchmann, J. Cerney, C. DeForest, D. Hunt, T. Jenness, T. Luka, R. Schwebel, and C. Soeller and can be obtained from <http://pdl.perl.org>

3. THE EXTINCTION TOWARDS CAS A

3.1. Reddening Measurements from Emission Lines

Reddening measurements of emission-line nebula require observations of at least two lines of known intrinsic ratio and significantly different energies. With the adoption of a reddening curve (e.g. Cardelli et al. 1989, which we use here) and an assumption about general-to-selective extinction ($R_V = A_V/E(B-V) = 3.1$ is the standard value for the diffuse ISM), the observed fluxes of the selected lines gives the extinction. $H\alpha$ and $H\beta$ (and higher order lines of the Balmer series) are most often used since they are generally among the brightest lines in nebular spectra and, in the usually applicable case where their emission is primarily by recombination, the intrinsic ratio is well-known. However, these lines are problematic in Cas A for two reasons. First, the fast-moving knots that dominate Cas A's optical spectra are composed of pure metals and are devoid of hydrogen lines. Second, while the quasi-stationary flocculi ("QSFs", shocked pre-SN circumstellar material) do emit in the Balmer series, the slow radiative shocks that illuminate these knots produce $H\alpha$ by both recombination and collisional excitation, making the intrinsic $H\alpha/H\beta$ (Balmer decrement) ratio uncertain. A value of 3.0 is usually assumed for radiative shocks, but this increases to slower shock speeds as collisional excitation becomes more important. HF96 report measurements of the Balmer decrement for two QSFs in Cas A, but regard their implied values ($A_V = 5.3, 6.2 \pm 0.9$) as upper limits.

Alternatively, it is possible to measure the extinction with metal line ratios. In the case where collisional de-excitation is negligible, the intrinsic flux ratio of lines originating from the same upper term depends only on their energies and transition probabilities. Unfortunately, calculation of the Einstein A coefficients for the forbidden lines most often observed in optical/IR emission-line nebula is a difficult task, and results can vary by 20% or more for different calculations of the same transitions. Moreover, if collisional de-excitation is important the intrinsic flux ratio depends both on the electron density and theoretically-calculated effective collision strengths, which may have systematic uncertainties equal to or greater than those of the transition probabilities.

The best extinction measurements for Cas A to date are from HF96, who examine the 1.03 μ m blend and $\lambda\lambda 4069, 4078\text{\AA}$ doublet of [S II], both of which originate in the 1P (second excited) term of S^+ . (Collisional de-excitation of these transitions is unlikely to be important in the Cas A FMK's, as their critical densities are of order 10^6 cm^{-3} .) The issue of the accuracy of the necessary atomic data is apparent in HF96, who assume a ratio 25% greater than had been used in an earlier study by Searle (1971). Aside from systematics related to the atomic data, two practical considerations limit the utility of the [S II] diagnostic. As noted above, the lines of interest originate from the second excited term of S^+ , so, unlike the ubiquitous [S II] $\lambda\lambda 6717, 6731\text{\AA}$ doublet, at lower temperatures it is possible to have a significant S^+ ionization fraction with little population of the higher term, resulting in weak lines. More importantly, the 4070 \AA lines are far into the blue, and are thus highly absorbed

towards Cas A. Indeed, for $A_V = 8$, the highest derived extinction inferred from the radio study of Troland et al. (1985), $A_{4070} > 11$. HF96 only report reddenings in the northeastern bright ring of Cas A, where the radio-inferred extinction is the least. This is likely a selection effect, as it becomes increasingly difficult to measure the faint 4070Å lines in heavily absorbed regions. Since radio studies show the reddening towards Cas A to be patchy and variable across the remnant, in order to constrain more tightly the extinction at the explosion it is highly desirable to be able to measure reddenings closer to the expansion center or, at least, sample a more representative range of sight lines.

With the general availability of efficient near-infrared spectrographs, it is now possible to observe a wider selection of emission lines into regions of higher extinction. The strong 1.257 μm and 1.644 μm lines of [Fe II] both originate in the $a^4D_{7/2}$ level of Fe^+ , are bright in a range of emission-line nebulae, and in principle should be ideal reddening indicators for moderately absorbed sources. However, the intrinsic flux ratio of these important lines is a matter of some debate. Two modern calculations of the relevant transition probabilities (Nussbaumer & Storey 1988 and Quinet et al. 1996) are discrepant by 30%. Because of the relatively small wavelength spacing of the two lines, this translates to a systematic error in A_V of several magnitudes. Hartigan et al. 2004 use the Quinet ratio ($F_{1.2575}/F_{1.644} = 1.04$) in their models, since it implies an A_V in HH111 that is consistent with optical Balmer decrement measurements (Gredel & Riepurth 1993). However, Nisini et al. (2005) find that neither the Quinet nor the Nussbaumer & Storey ratios produce A_V 's consistent with optical data in HH1. In light of such theoretical uncertainty, an empirical determination is desirable. To our knowledge, there are no published 1.257 μm /1.644 μm flux ratios for relatively unabsorbed sources (e.g.s. The Cygnus Loop or the Orion Nebula), but Smith & Hartigan (2006, hereafter SH06) present high S/N J and H band spectroscopy of P Cygni's nebula, and derive empirical Einstein A coefficients from their observations, using the known optical reddening. This is, of course, dependent on their assumed extinction ($A_V = 1.86$, Lamers et al. 1983), itself reliant on the accuracy of B star NLTE model atmospheres, being correct. However, given the current uncertainty in the actual intrinsic ratio, we accept the SH06 measurement ($F_{1.257}/F_{1.644} = 1.49$) as the best available, and use it throughout this work.

3.2. [Fe II] Reddening Measurements

We extracted numerous spectra from our coadded observations, seeking to maximize the signal to noise in the [Fe II] lines of interest. In Figure 2, we mark the positions of the 19 individual knots in which we measure the $F_{1.257}/F_{1.644}$ ratio to better than 20%. Of these, 16 are fast-moving ejecta knots and 4 are QSFs, located both in the northern bright ring (where HF96 made their measurements) and the more highly reddened western and southern portions of the remnant. In Figure 3, we show the measured flux ratio against position angle in the remnant. While there is considerable scatter due to Poisson noise in the lines, there is significant real variation on small spatial scales, as well as a general increase

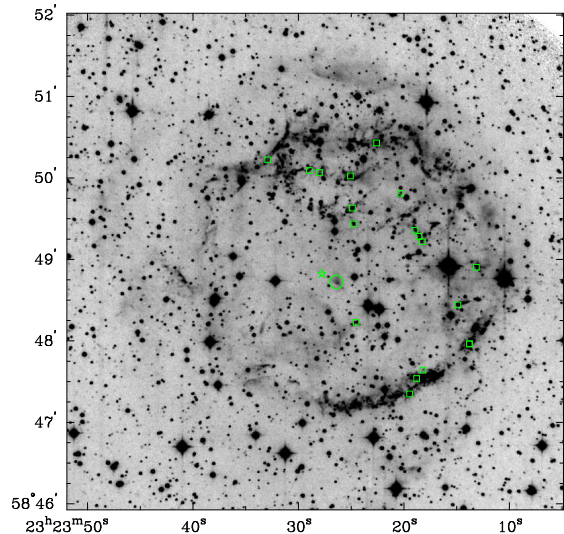


FIG. 2.— PISCES H band image of Cas A. Our knots with successfully measured [Fe II] ratios are marked with boxes, and synchrotron knot N is marked with a circle. The star symbol marks the expansion center as measured by Thorstensen et al. (2001).

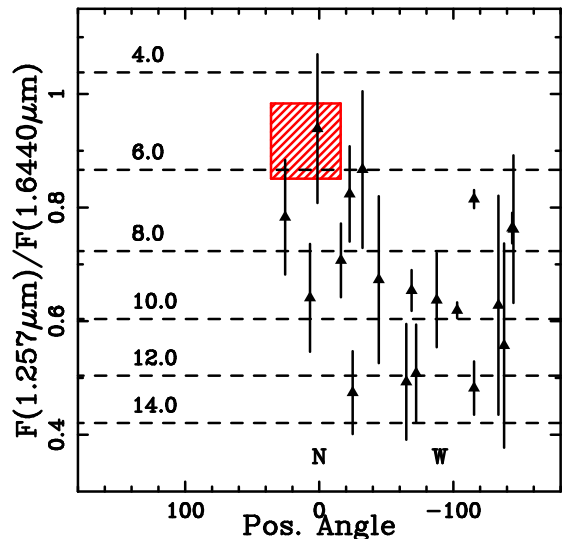


FIG. 3.— The observed flux ratios for 19 [Fe II] knots. The horizontal lines denote A_V assuming the empirical intrinsic flux ratio of Smith & Hartigan (2006). Adoption of the Nussbaumer & Storey (1988) ratio would decrease A_V by more than a magnitude. The hatched region shows the range of position angles sampled by HF96, and the range of reddenings from their optical [S II] lines.

in reddening from east to west. Both these attributes are broadly consistent with the radio measurements of Troland et al. (1985), who estimated $A_V \sim 4 - 5$ for much of the remnant, increasing to $A_V \sim 8$ in their western most observation. However, they argue that much of the molecular gas along the line of sight must be clumped in dark clouds smaller than their 1.1' beam, so the extinction would be expected to be greater in places, and vary on scales smaller than an arcminute.

Aside from the striking variation in reddening, an overall offset in the implied A_V as compared with the [S II] measurements from HF96 is clear. While there is no direct overlap in knots observed between the two samples, a number of our features are in the same area of the bright northern ring as the HF96 observations. Yet,

there is a marked difference of several magnitudes. The most likely explanation for this is the still quite uncertain atomic data for the forbidden lines of interest. A small portion of this error may come from the [S II] measurements. Our own calculation of the intrinsic [S II] ratio using more modern atomic rates (Keenan et al. 1993 and Keenan et al. 1996) suggests $F_{1\mu\text{m}}/F_{4070} = 0.58$, a revision down by approximately 10% compared with HF96’s adopted value. However, given the large separation in wavelength of the two blends, this only accounts for a few tenths of a magnitude in A_V . Rather, the likely culprit is the large uncertainty in the intrinsic relative strength of the two [Fe II] lines. Indeed, if we were to assume the theoretical value of Nussbaumer & Storey (1988) rather than the empirical ratio of SH06, the derived A_V would decrease by more than a magnitude, and would bring our least reddened values closer in line with HF96. This adjustment is problematic though, in that it would imply essentially zero extinction to P Cygni given SH06’s observed flux ratios, in conflict with ultraviolet and optical observations. Clearly, an empirical measurement on a less absorbed object is required to fix this distressing situation. Until its resolution, we caution that absolute measurement of A_V with these lines, for this SNR or any of the large number of astronomical objects that would benefit from NIR emission-line extinction diagnostics, requires better atomic data. However, apart from an absolute measurement, the variation in the observed flux ratio is a clear indication of the high spatial variation of the reddening toward Cas A, and demonstrates that an accurate estimate of the extinction of Cas A’s nascent supernova requires a measurement of A_V as close to the expansion center as possible. Our ability to reliably measure this ratio across the face of the remnant, even towards regions of comparatively high absorption, is a clear advantage over optical measurements.

Finally, we note the existence of two knots, one FMK and one QSF, within $45''$ of the measured expansion center of Cas A. The reddenings for these knots are $A_V = 7.4^{+2.1}_{-1.7}$ and $A_V = 6.0^{+1.9}_{-1.6}$ (statistical errors only). These are the closest emission line features to the projected explosion site to date with measured reddenings.

3.3. Reddening Measurement from Infrared Synchrotron Emission

Relativistic electrons accelerated in Cas A’s shocks produce copious amounts of synchrotron emission, and place Cas A among the brightest sources in the centimeter and millimeter sky. Cas A’s X-ray spectrum has a hard, broken power-law component (Allen et al. 1997) in addition to its thermal plasma signature, and *Chandra* has revealed a number of discrete filaments with featureless spectra (e.g. Hughes et al. 2000), which are generally assumed to be synchrotron emission (though, see also Laming 2001). It is then perhaps not surprising that synchrotron emission would be detected in the ~ 8 decades of energy in between. Gerardy & Fesen (2001) were the first to present high-quality near-infrared images of Cas A, and while their *J* band image was similar in morphology to clumpy, filamentary optical images dominated by emission lines, they noted the striking similarity of their K_s image to radio continuum maps, and postulated they had detected infrared synchrotron emission. Jones et al. (2003, hereafter J03) confirmed this iden-

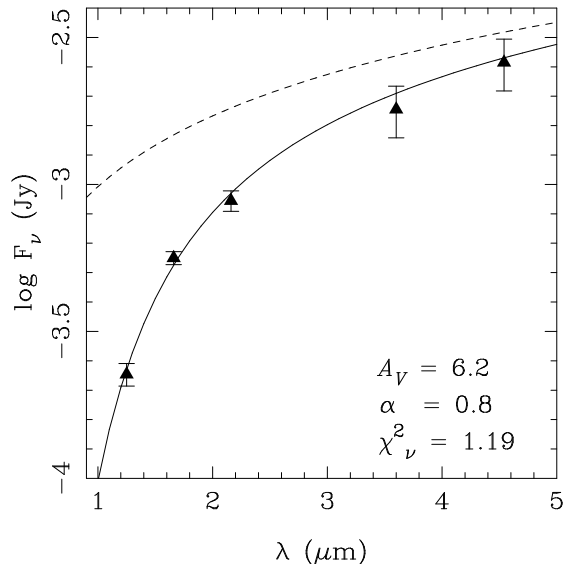


FIG. 4.— Measured infrared flux densities for Cas A synchrotron knot N. The solid line shows the best fit model for $A_V = 6.2$ and $\alpha = 0.80$, while the dashed line is the unabsorbed model.

tification with *K*-band imaging polarimetry of a small portion of the western shell. They also found the $2\mu\text{m}$ flux to be brighter than expected from simple extrapolation from the radio. Rho et al. (2003, hereafter R03) apparently confirm the “concave-up” nature of the Cas A synchrotron spectrum, though since their measurement is summed over the entire remnant, systematics like incomplete star subtraction, contamination from line-emission, spectral index variation, and large-scale flat field errors are likely sources of systematic error. Indeed, Wright et al. (1999, hereafter W99) show significant variation of spectral indices for several knots in the millimeter-wave regime.

Departures from a broadband power-law spectrum, either concave up or down, can be produced by a variety of plasma effects (e.g.s Eichler 1984, Reynolds 1998), and the detailed broadband shape of Cas A’s non-thermal SED is still an open question. Of course, at optical through mid-infrared wavelengths, the situation is complicated by the substantial extinction along our sight line to the remnant. (For $A_V = 4.5$ and a standard reddening law, $A_{4.5\mu\text{m}} = 0.16$ and is obviously greater for shorter wavelengths.) Here, we reverse the question: we assume the departure from a power-law is small over our limited range of energies, and determine A_V by fitting for the observed fall-off towards shorter wavelengths.

Practical measurement of the infrared synchrotron spectral index in Cas A is complicated in that in *J*, *H*, and IRAC channel 2, most regions of bright synchrotron emission are also bright in emission lines. However, a number of isolated continuum knots are line free. Fortunately, one of the brightest of these (“knot N” from W99, marked with a circle in Figure 2), is only $13''$ from Cas A’s expansion center (Thorstensen et al. 2001) making this the closest feature to the projected SN observed from the optical through mid-IR. Thus, a measurement of A_V at this location provides the strongest constraint on the actual reddening of Cas A’s SN.

In Figure 4, we plot the $1 - 5\mu\text{m}$ flux densities for a circular aperture of radius $10''$ centered on knot N, with

the background (determined from an annulus of inner radius $10''$ and outer radius $20''$) subtracted. For the ground-based JHK_s bands, we convert 2MASS magnitudes to Jy using the flux zero-points from the 2MASS documentation (Cutri et al. 2006). The error bars reflect the Poisson noise from the source and sky, and do not include any systematic error due to large-scale flat-field error or non-zero color terms in the flux calibration. We estimate these systematics to be sub-dominant. For the IRAC bands, flux density is a product of the post-BCD processing. The Poisson errors are negligible. However, due to the extended wings in the *Spitzer*/IRAC point-spread function, there is substantial systematic error in the flux densities. We correct the fluxes from the images down by 2% (ch1) and 5% (ch2), and assume a conservative 20% error in the absolute value ⁵.

In order to estimate A_V , we fit our data with a reddened power law and used a Markov Chain Monte Carlo (MCMC) technique to sample the three-dimensional parameter space of the fit. In Figure 5, we plot the likelihood contours in the $A_V - \alpha$ projection, marginalizing (i.e. integrating the likelihood function) over the normalization parameter. With flat priors on the parameters, there is a strong degeneracy between the extinction and spectral index, as higher A_V compensates for flatter spectra. This leads to only loose constraints on reddening. Indeed, the distribution of A_V marginalized over both α and k is quite broad and, without further constraints, we estimate $A_V = 7.9 \pm 1.9$.

The data and flat priors alone clearly allow non-physical values of the spectral index, and improbable reddenings. In order to limit the range of likelihood space available to the fit, it is clearly desirable to apply more stringent priors to the parameters. While one could choose somewhat arbitrary allowed ranges on the parameters (top-hat priors), we choose instead to apply a physically motivated prior on the spectral index, from the millimeter-wave radio observations. W09 report $\alpha = 0.80$ for knot N. While they do not quote an error specific to this knot, they claim their general accuracies to be $\pm 0.02 - 0.05$. We ran a second set of Markov chains with a Gaussian prior with $\sigma_\alpha = 0.05$. This shrinks the likelihood contours significantly, and tightly constrains the marginal probability distribution of the reddening (Figure 5). For this prior, we find $A_V = 6.2 \pm 0.6$.

Given the evidence for departures from a power-law in the broadband synchrotron spectrum of Cas A discussed previously, the actual uncertainty in the spectral index may indeed be greater than the statistical error quoted by W09. The concave-up spectra preferred by both J03 and R03 flattens the power-law, and would translate to a lower index in our model. Inspection of our likelihood contours shows that this would drive our fit to higher A_V . (Indeed, with the flat priors, our data prefers a flatter α and more extinction.) One could construct more exotic priors that preferentially open parameter space towards lower spectral indices, but absent a strong theoretical guide of their functional form, and given the relatively paucity of data points, we rapidly approach art over science. Shorter wavelength data, whose extinction increase faster than the intrinsic spectrum drops, may have power to constrain more tightly either the spectral index or any

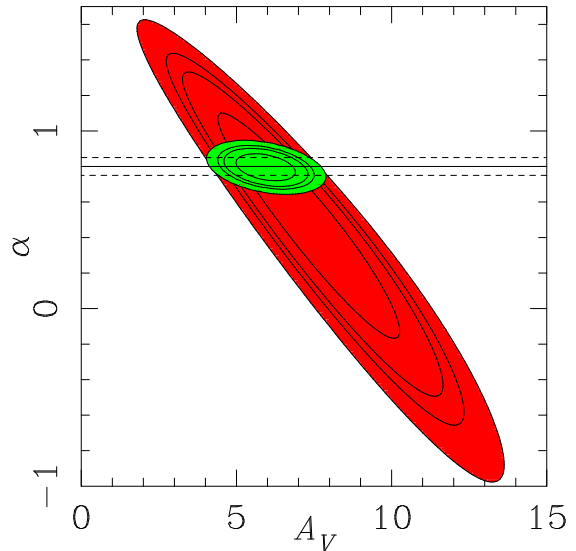


FIG. 5.— Likelihood contours for Cas A knot N for flat priors (red) and a Gaussian prior on the spectral index (green). The contours correspond to 68%, 90%, 95%, and 99% confidence for each set of priors. The horizontal line is the millimeter spectral index from Wright et al. (1999, solid), and their 1σ errors (dashed). significant departure from a power-law. Imaging of Cas A’s synchrotron emission should be feasible in the red end of the optical with moderate-sized telescopes. Ideally, one would like a $0.8 - 2.5\mu\text{m}$ dispersed spectrum of the emission, though this would require a significant investment of time on a large aperture facility.

4. DISCUSSION

4.1. Cas A’s Supernova at Maximum Light

Accepting our new extinction measurement from synchrotron knot N as the most likely A_V toward Cas A’s nascent supernova, we now seek to constrain a range of possible intrinsic peak luminosities, and therefore, ^{56}Ni yields. Following Young et al. (2006),

$$L_{\text{peak}} = M_{N_i} \Theta(t_{\text{peak}}) \Lambda(t_{\text{peak}}) \quad (1)$$

where M_{N_i} is the ejected mass of ^{56}Ni , $\Theta(t)$ is the instantaneous energy decay rate of ^{56}Ni and ^{56}Co , and $\Lambda(t)$ is the efficiency with which that energy is deposited in the supernova gas. $\Theta(t)$ is defined as

$$\Theta(t) = \frac{N_A}{56} \left[\frac{E_{N_i}}{\tau_{N_i}} e^{-t/\tau_{N_i}} + \frac{E_{Co}}{\tau_{Co} - \tau_{N_i}} \left(e^{-t/\tau_{Co}} - e^{-t/\tau_{N_i}} \right) \right]. \quad (2)$$

Here, N_A is Avogadro’s number, while E and τ are the γ -ray energy and mean decay lifetime of their respective nuclei (1.73 MeV and 7.6×10^5 s for nickel; 3.69 MeV and 9.6×10^6 s for cobalt). We choose $t_{\text{peak}} = 20.7$ days (the rise time for the SNIb 2008ax, Pastorello et al. 2008), and $\Lambda(t_{\text{peak}}) = 0.95$ (the value for the most likely Cas A progenitor from Young et al., determined with γ -ray radiative transfer calculations).

First, we estimate the minimum possible luminosity. Willingale et al. (2003) inventory $0.058 M_\odot$ (no error bar reported) of X-ray emitting iron in Cas A from X-ray observations, and conclude that most of this material is ejecta. Assuming plausible isotopic ratios, the vast majority of this material is ^{56}Fe , the stable daughter product

⁵ <http://ssc.spitzer.caltech.edu/irac/calib/extcal/index.html>

of ^{56}Ni . If we allow Willingale’s iron mass to be the sum total of ^{56}Ni ejected, the supernova’s absolute magnitude would be $M_V = -16.5$. At a distance of $3.4^{+0.3}_{-0.1}$ kpc, with $A_V = 6.2 \pm 0.6$, this translates to a peak apparent visual magnitude of $m_V = 2.3 \pm 0.7$. (We have included a 25% error in the X-ray emitting iron mass.)

Recently, Krause et al. (2008) observed the actual optical peak of Cas A’s supernova through a light echo, and definitively classified it as a rare Type IIb. They use the nearby SNIb SN1993J, which had a peak $M_V = -17.5$ (Richmond et al. 1994) as a template, assumed the maximum reddening ($A_V = 8$) inferred from the radio, and derived a peak visual magnitude of $m_V = 3.2$. Our study indicates the extinction is considerably less, with concomitant increase in apparent brightness. There is, however, significant variation in the peak luminosity of the peculiar SNIb class, with SN1996cb peaking at $M_V \approx -16.3$ (Qiu et al. 1999), so some care must be applied in treating the SNIb as a homogenous population.

Clearly, Flamsteed’s apparent observation of 3 Cas was not Cas A’s SN at maximum light, though it may have been the supernova in decline. Krause et al. note that their light echo grew fainter by a factor of 18 in 140 days and that this ~ 3 magnitude fading matches a similar decline in lightcurve of 1993J. Morgan (2008) explore the observability of the putative SN1680 with new atmospheric radiative transfer calculations and a detailed discussion of the timing within the year. We summarize his argument here, with our new extinction result. Given Flamsteed’s 16 August 1680 6^m observation, and our assumed peak apparent magnitude of $m \sim 1 - 3$, SN1680’s peak would have occurred in February-April. During this time, Cas A’s position would have transitted during daylight, and would not have been visible at maximum altitude by several magnitudes, given any of our estimates of its apparent magnitude. However, with Cassiopeia’s circumpolar location in the northern sky, SN1680 would still have been quite high in both the morning and evening twilight. If Cas A’s supernova were on the bright end of our estimates, while it may not have been visible during daylight like other historical supernovae, it would briefly have been one of the 20 brightest stars in the northern sky, and likely would have been reported. Conversely, if its peak magnitude were towards the fainter end of our range, it may have been just faint enough to escape notice.

4.2. ^{56}Ni and ^{44}Ti

Given our probable range of luminosity for the supernova, we now seek to bound the total mass of ejected ^{56}Ni . The detection of $0.058 M_\odot$ of iron in the X-ray sets a hard floor. It is more difficult to derive a stringent upper limit, given the lack of a rigorous detection threshold. A 0^m supernova would have garnered a great deal of contemporary attention; clearly Cas A’s supernova did not. Would a 2^m or 3^m transient escape notice? Absent a clear answer, with the definition of the distance modulus and inverting equation (1)

$$M_V = m_v - A_V - \mu \propto \log_{10} M_{Ni} \quad (3)$$

we combine our ignorance into the $m_V - A_V$. In Figure 6, we plot this difference against the calculated ejected mass of nickel. The lower limit on M_{Ni} , combined with

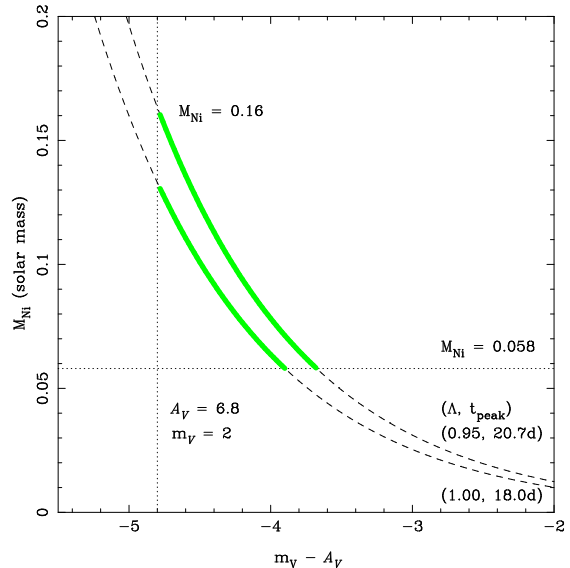


FIG. 6.— ^{56}Ni mass for two sets of assumptions for the supernova rise time and efficiency of γ -ray energy deposition. The horizontal dotted curve denotes the X-ray emitting iron mass, while the vertical dotted line represents the brightest plausible optical transient that might be missed ($m_V = 2$), and our best fit $A_V + 1\sigma$. The green solid line marks the allowed range of ^{56}Ni mass.

our best fit A_V implies $m_V < 2.4$. This is uncomfortably bright, but not an entirely unreasonable magnitude for an object that may have gone unnoticed in the twilight. If, instead we assume at 1σ increase over our best A_V and assume that any transient with $m < 2$ would merit at least a historical footnote, we place an upper limit on $M_{Ni} < 0.16 M_\odot$. We regard this as a conservative estimate. Plausibly shorter rise times and larger energy deposition efficiencies can lower this limit by $\sim 20\%$.

Gamma-ray observations have detected the nuclear decay lines of ^{44}Ti daughter nuclei ^{44}Ca and ^{44}Sc (Iyudin et al. 1994, Vink et al. 2001). The latest γ -ray observations imply an initially synthesized ^{44}Ti mass of $1.6^{+0.6}_{-0.3} \times 10^{-4} M_\odot$ (Renaud et al. 2006), for a $^{44}\text{Ti}/^{56}\text{Ni} = 0.8 - 3.8 \times 10^{-3}$. This high mass and ratio is problematic for spherically symmetric explosion calculations (Timmes et al. 1996), though in multi-dimensional asymmetric simulations some mix of differentially enhanced α -rich freezeout (Nagataki et al. 1998) and differential fallback (Young et al. 2006) appear capable of reproducing a range of yields, some consistent with the observed value. Notably, the combination of the new *INTEGRAL* titanium measurements and our tighter bound on the ejected ^{56}Ni mass shrink considerably the allowed abundance ratio space considered by Young et al (2006), and may provide important constraints on advanced supernova explosion calculations. Finally, we note that our radioactive Ti/Ni bound is consistent with the solar $^{44}\text{Ca}/^{56}\text{Fe}$ ratio (1.5×10^{-3} , Anders & Grevesse 1989) the stable isotopes of the considered decay chains. While it is dangerous to extrapolate from one observation, if this result is generally valid, Cas A-like supernovae may lessen the need for the sub-Chandrasekhar mass SNIa required by Timmes et al. (2006) to match the solar abundance.

Finally, we note an alternative explanation for the apparent faintness of Cas A’s supernova. While nearly all long duration gamma-ray bursts show late-time su-

pernova light curves, a small number do not (e.g. GRB060606 and GRB060615, Fynbo et al. 2006). Calculations by Fryer et al. (2007) show that sufficiently delayed explosions (after core collapse) produce a large mass of material on gravitationally bound ballistic trajectories, which falls back onto the compact remnant (a black hole for GRBs) on a timescale of minutes after the explosion. A correspondingly small amount of nickel escapes into the remnant. In these cases, the lightcurve is powered not by radioactive decay, but by energy deposited by the blast wave. These supernova are fainter and decline faster. In principle, similar such delayed supernovae could exist independently of GRBs, and their outbursts would be easier to hide. This idea is attractive in that the spectra of a number of the oxygen-rich supernova remnants lack iron, or even oxygen-burning ashes such as sulfur, argon, and calcium (e.g. N132D and E0102, Blair et al. 2000), which may well have fallen back onto the compact remnant. However, given the significant mass of iron detected in the X-ray spectrum of Cas A, its supernova was unlikely to have been such an event, so interstellar extinction remains the likely culprit in its apparent faintness.

5. CONCLUSION

We have presented new extinction measurements for Cassiopeia A that show the reddening to be more variable and of higher magnitude than had been derived from previous optical measurements, though our estimates of A_V are consistent with previous radio observations. The

[FeII] lines should be promising probes of reddening for regions of moderate extinction, though their use is still hampered by uncertainty in the intrinsic emissivity ratio of the two lines. Further atomic structure calculations, or more appropriately, observations of unabsorbed emission line sources are necessary to yield the full utility of these features. Nevertheless, the observed ratio is sufficient to show the east-west reddening gradient previously inferred in the radio, as well as small scale point-to-point variations.

We have also shown that estimation of A_V from the infrared synchrotron index combined with constraints from the radio yields statistical errors comparable to or better than those from the emission lines. Fortunately, a bright synchrotron knot free from emission-line contamination is located just $13''$ away from the derived expansion center of the remnant, and thus provides the strongest constraint on A_V toward Cas A's nascent supernova. Our new reddening, taken with the lack of widespread reportage of the supernova and with an iron mass inventory from the X-ray, bounds the ejected mass of ^{56}Ni to be $0.058 - 0.16M_\odot$. This nickel abundance and measurement of the ^{44}Ti yield from γ -radiation both provide constraints on possible asymmetry in the supernova explosion, and imply a $^{44}\text{Ca}/^{56}\text{Fe}$ ratio consistent with solar, which may have consequences for Galactic chemical evolutionary models.

Facilities: Bok (PISCES imager), Mayall (FLAMINGOS spectrograph), Spitzer (IRAC imager)

REFERENCES

- Allen, G. E., et al. 1997, ApJ, 487, L97
 Anders, E., & Grevesse, N. 1989, Geochim. Cosmochim. Acta, 53, 197
 Ashworth, W. B., Jr. 1980, Journal for the History of Astronomy, 11, 1
 Blair, W. P., et al. 2000, ApJ, 537, 667
 Bohlin, R. C. 2007, The Future of Photometric, Spectrophotometric and Polarimetric Standardization, 364, 315
 Cardelli, J. A., Clayton, G. C., & Mathis, J. S. 1989, ApJ, 345, 245
 Cutri, R. M., et al. 2006, Explanatory Supplement to the 2MASS All Sky Data Release and Extended Mission Products, <http://www.ipac.caltech.edu/2mass/releases/allsky/doc/explsup.html>
 Eichler, D. 1984, ApJ, 277, 429
 Ennis, J. A., Rudnick, L., Reach, W. T., Smith, J. D., Rho, J., DeLaney, T., Gomez, H., & Kozasa, T. 2006, ApJ, 652, 376
 Fesen, R. A., Pavlov, G. G., & Sanwal, D. 2006, ApJ, 636, 848
 Fynbo, J. P. U., et al. 2006, Nature, 444, 1047
 Fryer, C. L., Hungerford, A. L., & Young, P. A. 2007, ApJ, 662, L55
 Gredel, R., & Reipurth, B. 1993, ApJ, 407, L29
 Gerardy, C. L., & Fesen, R. A. 2001, AJ, 121, 2781
 Gray, R. O., & Corbally, C. J. 1994, AJ, 107, 742
 Hartigan, P., Raymond, J., & Pierson, R. 2004, ApJ, 614, L69
 Hughes, J. P., Rakowski, C. E., Burrows, D. N., & Slane, P. O. 2000, ApJ, 528, L109
 Hurford, A. P., & Fesen, R. A. 1996, ApJ, 469, 246
 Iyudin, A. F., et al. 1994, A&A, 284, L1
 Jones, T. J., Rudnick, L., DeLaney, T., & Bowden, J. 2003, ApJ, 587, 227
 Kamper, K. W. 1980, The Observatory, 100, 3
 Keenan, F. P., Hibbert, A., Ojha, P. C., Conlon, E. S. 1993, Phys. Scr, 48, 129
 Keenan, F. P., Aller, L. H., Bell, K. L., Hyung, S., McKenna, F. C., & Ramsbottom, C. A. 1996, MNRAS, 281, 1073
 Keohane, J. W., Rudnick, L., & Anderson, M. C. 1996, ApJ, 466, 309
 Glazebrook, K., & Economou, F. 1997, Dr. Dobb's Journal, 9719, 45
 Krause, O., Birkmann, S. M., Usuda, T., Hattori, T., Goto, M., Rieke, G. H., & Misselt, K. A. 2008, Science, 320, 1195
 Lamers, H. J. G. L. M., de Groot, M., & Cassatella, A. 1983, A&A, 128, 299
 Laming, J. M. 2001, ApJ, 546, 1149
 McCarthy, D. W., Jr., Ge, J., Hinz, J. L., Finn, R. A., & de Jong, R. S. 2001, PASP, 113, 353
 Morgan, J. A. 2008, The Observatory, 128, 80
 Nagataki, S., Hashimoto, M.-A., Sato, K., Yamada, S., & Mochizuki, Y. S. 1998, ApJ, 492, L45
 Nisini, B., Bacciotti, F., Giannini, T., Massi, F., Eisloffel, J., Podio, L., & Ray, T. P. 2005, A&A, 441, 159
 Nussbaumer, H., & Storey, P. J. 1988, A&A, 193, 327
 Pastorello, A., et al. 2008, MNRAS, 389, 955
 Qiu, Y., Li, W., Qiao, Q., & Hu, J. 1999, AJ, 117, 736
 Quinet, P., Le Dourneuf, M., & Zeppen, C. J. 1996, A&AS, 120, 361
 Reynoso, E. M., & Goss, W. M. 2002, ApJ, 575, 871
 Rho, J., Reynolds, S. P., Reach, W. T., Jarrett, T. H., Allen, G. E., & Wilson, J. C. 2003, ApJ, 592, 299
 Reed, J. E., Hester, J. J., Fabian, A. C., & Winkler, P. F. 1995, ApJ, 440, 706
 Reynolds, S. P. 1998, ApJ, 493, 375
 Richmond, M. W., Treffers, R. R., Filippenko, A. V., Paik, Y., Leibundgut, B., Schulman, E., & Cox, C. V. 1994, AJ, 107, 1022
 Rousselot, P., Lidman, C., Cuby, J.-G., Moreels, G., & Monnet, G. 2000, A&A, 354, 1134
 Searle, L. 1971, ApJ, 168, 41
 Skrutskie, M. F., et al. 2006, AJ, 131, 1163
 Smith, N., & Hartigan, P. 2006, ApJ, 638, 1045
 Timmes, F. X., Woosley, S. E., Hartmann, D. H., & Hoffman, R. D. 1996, ApJ, 464, 332
 Thorstensen, J. R., Fesen, R. A., & van den Bergh, S. 2001, AJ, 122, 297
 Troland, T. H., Crutcher, R. M., & Heiles, C. 1985, ApJ, 298, 808

- Vink, J., Laming, J. M., Kaastra, J. S., Bleeker, J. A. M.,
Bloemen, H., & Oberlack, U. 2001, ApJ, 560, L79
- Willingale, R., Bleeker, J. A. M., van der Heyden, K. J., &
Kaastra, J. S. 2003, A&A, 398, 1021
- Wright, M., Dickel, J., Koralesky, B., & Rudnick, L. 1999, ApJ,
518, 284
- Young, P. A., et al. 2006, ApJ, 640, 891